JOURNAL OF MATERIALS SCIENCE 30 (1995) 784–792

Calculation of CO_2 laser beam absorptance as a function of temperature for steels by the numerical method

T. H. KIM, K. C. CHONG, B. Y. YOO
Department of Metallurgical Engineering, Yonsei University, Seoul 120-749, Korea
J. S. LEE
Department of Mechanical Engineering, Seoul National University, Seoul 151-742, Korea
K. H. WHANG
Korea Institute of Machinery and Metals, Changwon 641-010, Korea

Temperature distributions were measured during the irradiation of a CO_2 laser beam at one end of a rod-shaped specimen and at the centre of a thin plate-shaped specimen. Regarding the measured temperature distributions as one-dimensional and two-dimensional unsteady state heat transfer solutions, CO_2 laser beam absorptances were calculated using a modified finite difference method. Temperature dependence of thermal properties, heat loss due to convection and latent heat during melting of the specimen were taken into account in this numerical calculation. Increasing the specimen temperature from room temperature to melting point, absorptances of STS304 stainless steel and SM45C steel were calculated as 8 ~ 40% and 6 ~ 41% for the one-dimensional calculation, and as 9.3 ~ 41% and 5 ~ 41% for the two-dimensional calculation, respectively. These calculated absortances were very close to theoretical values at relatively low temperature, which were calculated from the electrical resistivities of the specimens. Increasing the temperature of the specimens, absorptances increased considerably due to oxidation of the specimens. Regardless of specimen composition and specimen dimension, both absorptances showed nearly the same value of 41% at their melting points, in which the structures of both metals became amorphous phases.

1. Introduction

In material processing by laser beams, probably the most important single parameter is the absorptance of the laser beam on the material's surface, since the basic mechanisms of laser material processing are heating, melting and evaporation of material by the absorbed laser beam. Therefore, it is necessary to know accurately the absorptance of the laser beam on the material's surface for control of laser material processing. Especially, the absorptance of the laser beam on the melted-state steel is very important for surface-alloying, welding and cutting.

Generally, laser beam absorptance is obtained by measurement of reflectance on the material's surface using photodiode or calorimetric methods. However, it is difficult to use a photodiode for reflectance measurement of the CO_2 laser beam, since its wavelength belongs to the far infrared (i.r.) range. For the calorimetric method, in order to analyse the heat balance problem, it is necessary to consider the temperature dependence of thermal properties in the materials, ejection of molten metal, evaporation and plasma formation, during irradiation of the high power laser beam on the surface. Nevertheless, in order to acquire laser beam absorptance for the high power laser beam, most investigators apply the calorimetric method, by assuming some conditions in which the absorbed energy is measured and compared with incident laser energy.

A CO_2 laser beam absorptance of 9–11% has been reported for stainless steel, depending upon the temperature when the specimen was solid [1]. If the CO_2 laser beam intensity is high enough to melt various steels and to form a keyhole on the specimen, absorptances of 50–95%, as shown on Table I, depending upon the specimen and laser irradiation condition have been reported [2–10].

In most of these experiments, one or two thermocouples were used to measure the temperature of the whole specimen, and average thermal properties were used and various heat losses were disregarded in absorptance calculations. However, since the laser beam is irradiated on a local area in real cases, the temperature distribution is not uniform throughout the specimen and the thermal properties change during heating, and various heat losses are possible.

0022–2461

TABLE I Measured CO_2 laser beam absorptance

Absorptance (%)	Materials and welding condition	Reference
90	12.5 mm steel	2
95	Steel, 3 kW, 10 mm s^{-1}	3
60, 75	0.8 mm, 1.0 mm stainless steel, 1 kW, 10 mm s^{-1}	4
50	Steel, 3.8 kW	5
75	Mild steel, 11 kW, 5 mm s^{-1}	6
66	12.7 mm A36 steel, 12 kW, 12.7 mm s^{-1}	7
50	10 mm BS4630 50D steel, 4.5 kW, 5 mm s^{-1}	8
70, 80	Mild steel, 304 stainless steel, 3 kW, 3 m min^{-1}	9
65	Mild steel, 2 kW, 20 mm s^{-1}	10

Therefore, it is necessary to consider more detailed temperature distributions, a transient temperature increase and heat losses in order to calculate more accurate absorptance values.

In this research work, in order to obtain accurate absorptances of the CO_2 laser beam on stainless steel and medium carbon steel at various temperatures, the numerical calculation method was applied for both one-dimensional and two-dimensional specimens. For the one-dimensional specimen, the temperature distribution was measured during irradiation of the CO_2 laser beam at one end of a rod-shaped specimen. Regarding the measured temperature distribution as a one-dimensional unsteady state heat transfer solution, the CO_2 laser beam absorptance was calculated quantitatively using a modified finite difference method [11]. For the two-dimensional specimen, the temperature distribution was measured during irradiation of the laser beam on one side of a thin plate-shaped specimen. Regarding the measured temperature distribution as a two-dimensional unsteady state heat transfer solution, laser beam absorptance was calculated by the same method [12]. Then, these results were compared.

In order to determine the temperature dependence of laser beam absorptance on the specimen, laser beam power was varied in this experiment: 50 W, at which temperature the specimen did not melt, and 750 W, which was enough to melt the specimen. Temperature dependence of the thermal properties and heat loss due to convection were taken into account in this numerical calculation. Absorbed energy during irradiation of the laser beam was regarded as generated energy in the first mesh layer near the specimen surface. Latent heat of the specimen during melting was treated with the temperature recovery method, and thermal conductivity was revised to effective thermal conductivity in the melted region for calculation. This numerical calculation allows a solution to the unsteady state heat transfer problem and offers a simple method to obtain accurate absorptance of the laser beam on the metal.

2. Experimental procedure

2.1. Materials and laser irradiation

Specimens used in this work were STS304 stainless steel (0.08 wt% C, 18.0 wt% Cr, 8.0 wt% Ni, 2.0 wt% Mn, 0.75 wt% Si, balance Fe) and SM45C steel (0.45 wt% C, 0.75 wt% Mn, 0.25 wt% Si, balance Fe). Rod-shaped specimens of 5 mm diameter and 100 mm length, and plate-shaped specimens of 0.5 mm thickness and 150 × 150 mm area were used. In order to obtain accurate absorptance, the region where the laser beam was irradiated was polished with diamond paste. For specimens whose surfaces were not melted, CO_2 laser power was about 50 W and the irradiation time was 5–30 s. For specimens whose surfaces were melted, these values were about 750 W and 1–5 s. The laser beam was TEM_{01}* mode. During laser irradiation on the specimen, shielding gas was not applied to the specimen in order to suppress convection heat loss. Since the experiment was carried out in an atmospheric environment, oxidation on the surface could not be neglected during laser irradiation. Thus, oxidation phenomena of both specimens were checked up to 1000 °C using thermogravimetric differential thermal analysis (TGA-DTA) equipment.

2.2. Temperature measurement

In order to measure temperature distribution in one-dimensional specimens, thermocouples were spot-welded at four locations along each specimen, as shown in Fig. 1. The spot size of the laser beam was chosen to be 5 mm, in accordance with the specimen diameter.

For the two-dimensional specimen, thermocouples were spot-welded at four locations beneath the specimen, as shown on Fig. 2. The spot size of the laser beam was chosen to be 2 mm in order to give convenient numerical calculation. If the spot size was too small, then the mesh size would be small and, also, the time step would be small too, in the numerical calculation.

Thermocouples used in this work were K-type (chromel–alumel), with diameters of 0.2 mm. The electromotive force (e.m.f.) generated in the thermocouples during irradiation of the laser beam was measured by an a.c./d.c. converter every 0.02 s, and then converted into temperature using a personal computer.

The experimentally measured temperature distribution was compared with what was calculated by putting an arbitrary laser absorptance value into the

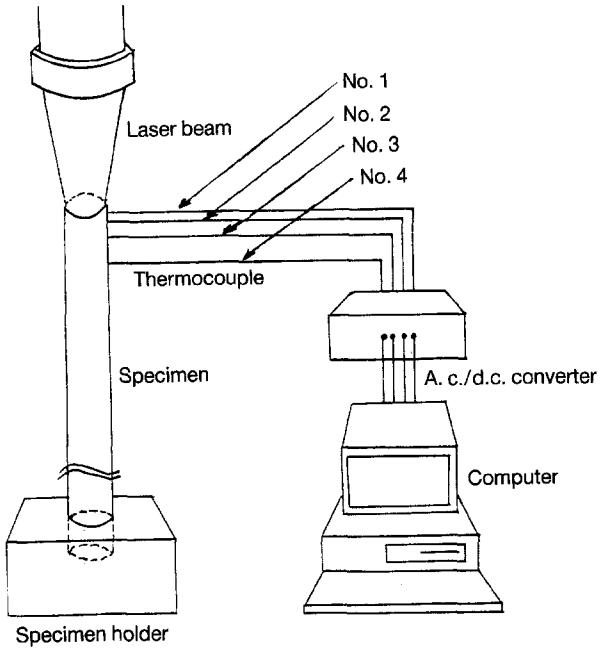

Figure 1 Schematic diagram of laser irradiation and temperature measurement for the one-dimensional model.

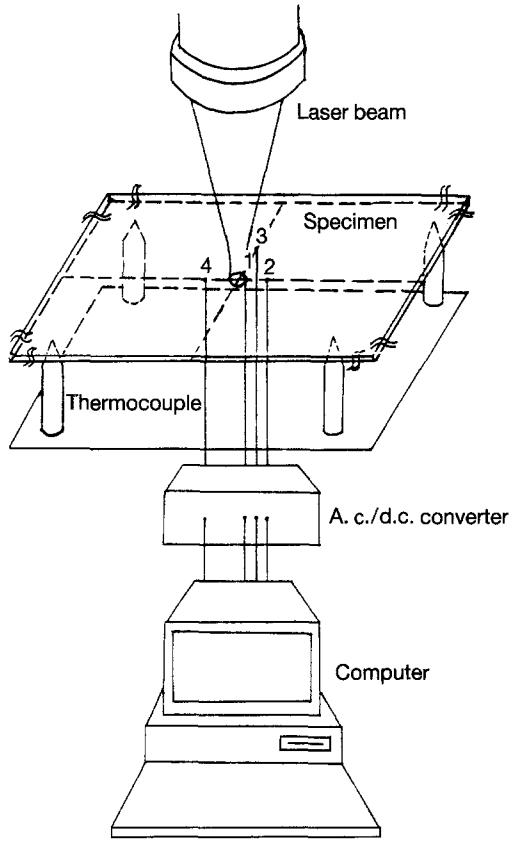

Figure 2 Schematic diagram of laser irradiation and temperature measurement for the two-dimensional model.

numerical method. If this calculated temperature distribution agreed well with the measured one, then this arbitrary input value was taken as the calculated absorptance. If both temperature distribution curves deviated from one another, then other arbitrary values were substituted in this calculation until the calculated temperature distribution fitted the measured one.

3. Numerical analysis model

3.1. Heat transfer differential equation

When the CO_2 laser beam was irradiated at one end of the rod-shaped specimen, with length, L, the one dimensional unsteady state heat transfer differential equation was given by the following

$$\rho C_p \frac{\partial T}{\partial t} = \frac{\partial}{\partial t}\left(K\frac{\partial T}{\partial z}\right) + Q_1 \quad (0 \le z \le L)$$

$$Q_1 = h(T_a - T_s)$$

For the initial condition

$$T = T_0, \qquad t = 0$$

For the boundary condition

$$q = A\frac{P}{\pi r^2}, \qquad z = 0$$

$$T = T_0, \qquad z = L$$

For a thin plate-shaped specimen, the two-dimensional unsteady state the heat transfer differential equation was given by cylindrical co-ordination with equivalent initial and boundary conditions

$$\rho C_p \frac{\partial T}{\partial t} = \frac{1}{r}\frac{\partial}{\partial t}\left(r \times K\frac{\partial T}{\partial r}\right) + \frac{\partial}{\partial z}\left(K\frac{\partial T}{\partial z}\right) + Q_1$$

where ρ is the density; C_p, specific heat; K, thermal conductivity; Q_1, heat loss due to convection and radiation; h, heat transfer coefficient due to convection and radiation; T_a, atmospheric temperature; T_s, specimen surface temperature; T_0, specimen initial temperature; q, thermal flux on boundary surface; A, laser beam absorptance; P, laser beam power; r, radius.

In numerical calculation of the one-dimensional unsteady state heat transfer problem, assumptions were as follows.

1. Laser beam power was constant during the irradiation period, and the laser beam was the surface heat source on the irradiated area.
2. Temperature gradient was neglected in a radial direction during irradiation of the laser beam.
3. Thermal conductivity and specific heat of the specimen were functions of temperature, and density was constant.

The first assumption was quite possible, since the skin depth where laser energy was converted into thermal energy was several hundred nm, and this was quite smaller than the diameter of the specimen. The second assumption was possible due to the fact that the Biot number was 0.001 25 in this experimental condition. The Biot number represents the degree of temperature gradient in the material, and it is given by $\mathrm{Bi} = h \times r/2K$ for the rod-shaped specimen, where h, r, K are as given previously. If the Biot number is smaller than 0.1, then the temperature gradient is not important [13]. The third assumption originated from the fact that the thermal properties of the materials were dependent upon temperature, while density did not change much during melting.

For the two-dimensional case, some more assumptions were made, in addition to the general assumptions given above.

1. Since the laser beam was cylindrically symmetric, the temperature did not change along the θ-direction.
2. If the laser beam was irradiated for a short period, the laser beam caused rapid heating, and the local heated area was very small compared to the whole specimen area. Thus, the analysis model was assumed to be a radially semi-infinite material model from the laser irradiated area.

3.2 Discritization of differential equation and computer program

In the heat conduction problem, the discritization equation can be obtained directly from the energy conservation law of finite elements. Thus, the related system in this work was divided into many small elements. From physical phenomena and energy conservation of each element, a discritization equation was obtained using the modified finite difference method, which can carry out numerical calculation. In order to calculate the temperature distribution by the discritization method, the outer nodal point method was applied for location and area of the nodes, and then the advanced modified finite difference method was introduced.

Fig. 3 shows the system model and divided elements in the one-dimensional rod-shaped specimen.

For two-dimensional analysis, it was reported that at least five meshes should be located inside the beam spot in order to represent the transverse mode of the laser beam [14]. If a homogeneous mesh size was applied in the whole specimen, the number of meshes would be too large to calculate by personal computer, since the spot size of the laser beam was chosen to be 2 mm in this thin plate-shaped specimen. Therefore, variable meshes were introduced in this calculation, as shown on Fig. 4, where mesh size increased gradually from the centre to the outer region [14–16].

Here, although variable meshes were used for radial direction, homogeneous meshes were used for the Z-direction, since the thickness of the specimen was 0.5 mm, which was very thin compared with the dimensions of the whole specimen.

For an arbitrary time step, the general energy conservation law is as follows

$$\Delta E_{st} = E_{in} + E_g - E_{out}$$

where ΔE_{st} is the stored energy in controlled volume; E_{in}, the input energy in controlled volume; E_g, the generated energy in controlled volume; E_{out}, the output energy in controlled volume.

Specimen dimension, laser beam power, initial temperature, time step and arbitrary absorptance were put into the computer program, and then the temperature of each element was calculated repeatedly for each time step by the discritization method. If the calculated temperature was above the melting point, the temperature recovery method was applied in the treatment of latent heat, and effective thermal conductivity was used to modify convection of the melt

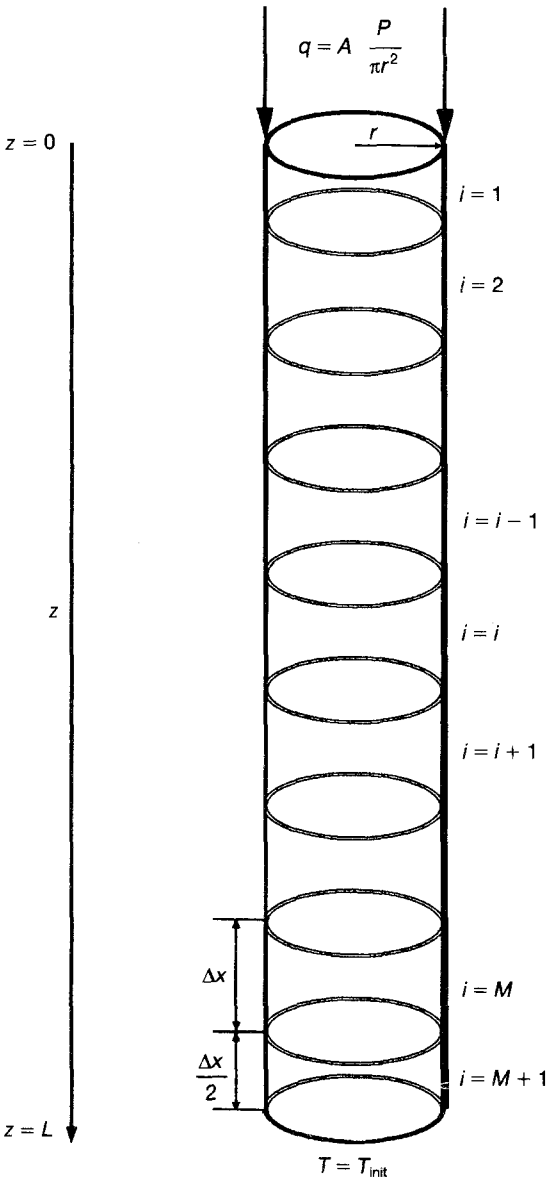

Figure 3 Schematic diagram of the one-dimensional model system for computer simulation and generalized finite difference meshes for computer analysis.

[17]. If the temperature distribution calculated by the above method did not accord with that measured experimentally, new absorptance values were substituted into the input data, repeatedly, until both temperature distributions accorded with each other. The above heat conduction differential equation is effective only if thermal conductivity and specific heat are constant. However, these values are functions of temperature [18]. Nevertheless, these values can be assumed to be constants within each time step, if new thermal conductivity and specific heat values, corresponding to specimen temperature, were substituted in each time step, repeatedly. Thus, there was no problem in using the above equation to calculate temperatures. Thermal conductivity and specific heat were calculated for each time step by a subroutine program which was then introduced into the main program. Also, the heat transfer coefficient was calculated for each time step for corresponding specimen

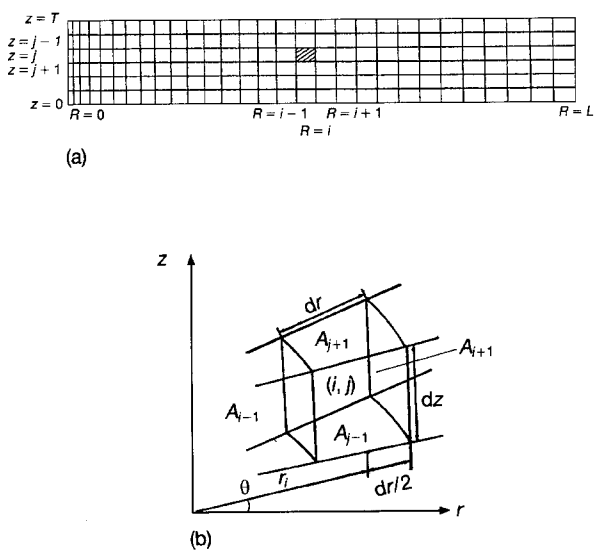

Figure 4 Schematic diagram of the two-dimensional model system for computer simulation: (a) variable meshes for computer analysis, (b) schematic drawing of nodal points in one element for the modified finite difference method.

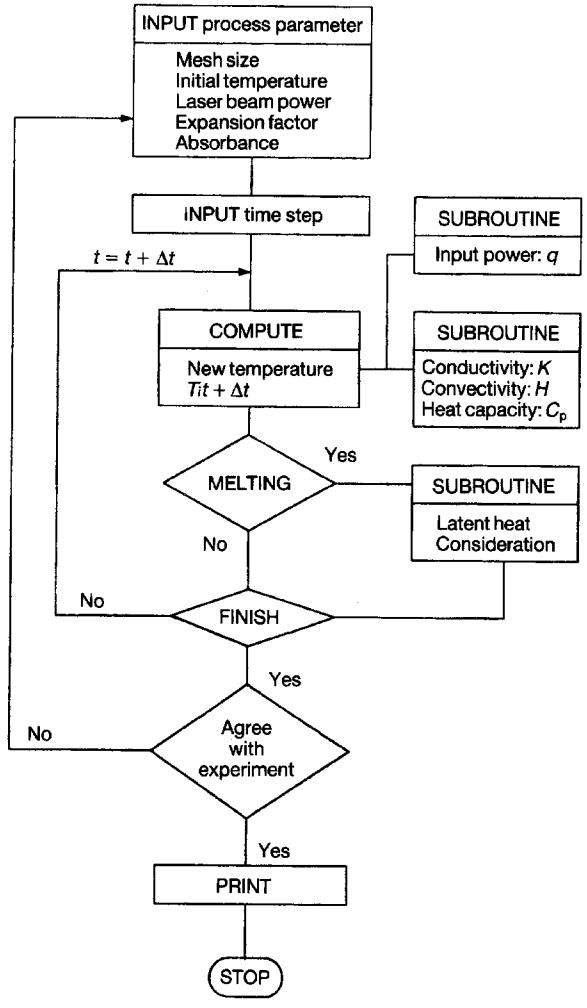

Figure 5 Simplified flow chart of computer program.

temperature, and the laser energy density on local area spot size was calculated.

Fig. 5 is a flow chart representing the computer programming for this calculation.

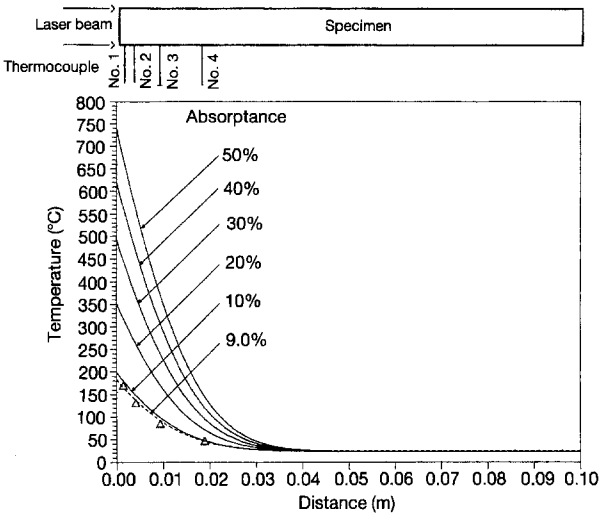

Figure 6 Measured (△) and predicted (—) temperatures for one-dimensional STS304 stainless steel specimen (laser power, 48 W; irradiation time, 30 s).

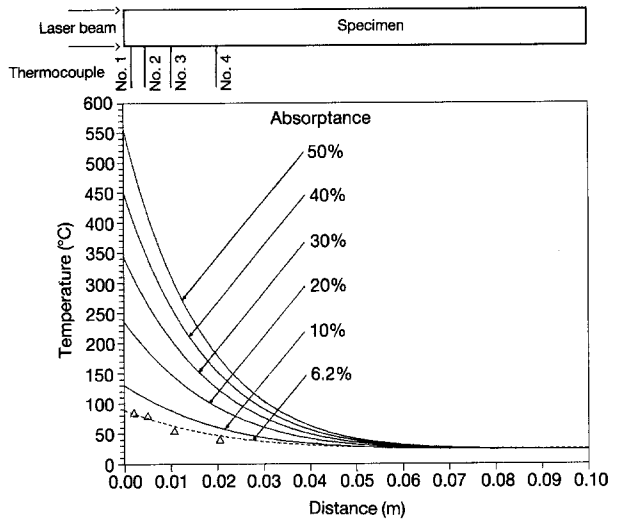

Figure 7 Measured (△) and predicted (—) temperatures for one-dimensional SM45C steel specimen (laser power, 48 W; irradiation time, 30 s).

4. Results and discussion

4.1. Low power laser beam for non-melting specimens

Figs 6 and 7 show the temperature distributions of STS304 stainless steel and SM45C steel when the laser beam power was 48 W and the irradiation time was 30 s for one-dimensional cases. Here, the solid lines represent the numerically calculated temperature distributions if laser absorptances were assumed to be 50, 40, 30, 20 and 10%, respectively. The dotted lines represent those values when absorptances were assumed to be 9.0% for STS304 stainless steel and 6.2% for SM45C steel. These dotted lines fitted quite well with experimentally measured temperatures.

Figs 8 and 9 show the temperature distributions of STS304 stainless steel and SM45C steel when the laser power was 82 W and irradiation time was 2 s for two-dimensional cases. Here, the solid and dotted lines can be interpreted as in Figs 6 and 7.

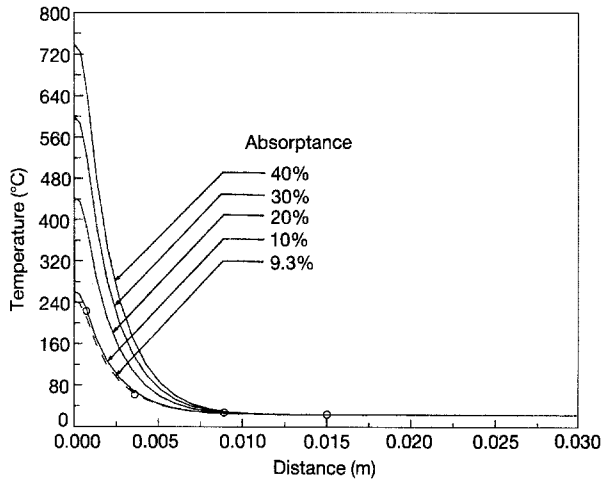

Figure 8 Measured (○) and predicted (—) temperatures for one-dimensional STS304 stainless steel specimen (laser power, 82 W; irradiation time, 2 s).

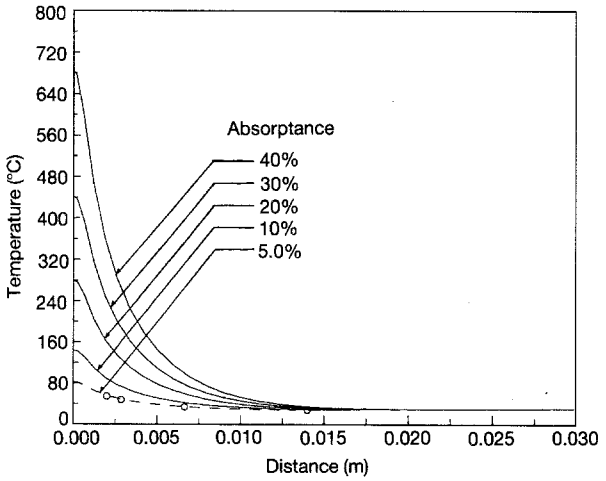

Figure 9 Measured (○) and predicted (—) temperatures for one-dimensional SM45C steel specimen (laser power, 82 W; irradiation time, 2 s).

Electromagnetic wave reflectance on metal can be calculated theoretically, if the electrical resistivity of the metal is given [19, 20]. The reflectance of the laser beam increases if the electrical resistivity of the metal decreases. The electrical resistivity of STS304 stainless steel is higher than that of SM45C steel, thus the absorptance of the laser beam on STS304 stainless steel was higher than that of SM45C steel as expected. These numerically calculated absorptances were very close to the theoretically calculated and other experimentally measured values. If the temperature of the specimen is increased by extending laser irradiation time, electrical resistivity also increases. Then, more laser energy is absorbed on the surface due to reduction of reflectance. Since the temperature on each location increased accordingly as laser irradiation time was extended, the calculated laser absorptance increased from 8.1 to 9.0% for STS304 stainless steel and from 6.0 to 6.2% for SM45C steel as the irradiation time increased from 5 s to 30 s for the one-dimensional case, as shown in Figs 10 and 11.

For the two-dimensional case, the absorptance increased from 9.3 to 11.1% for STS304 stainless steel

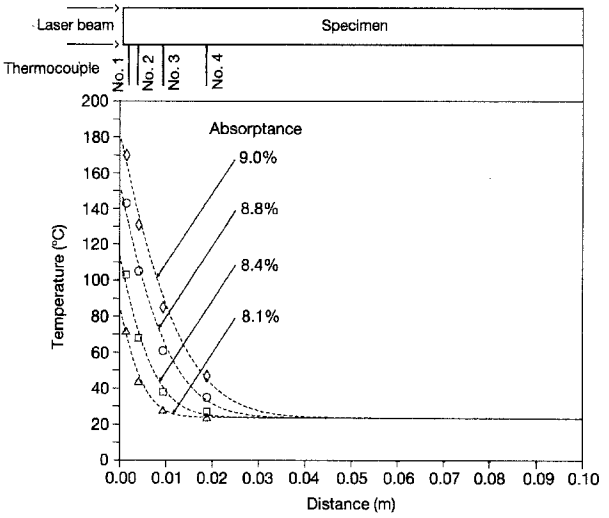

Figure 10 Measured temperature, simulated temperature and calculated absorptances as a function of laser irradiation time for one-dimensional STS304 stainless steel specimen (laser power, 48 W). For: (◇) 30 s, (○) 20 s, (□) 10 s and (△) 5 s.

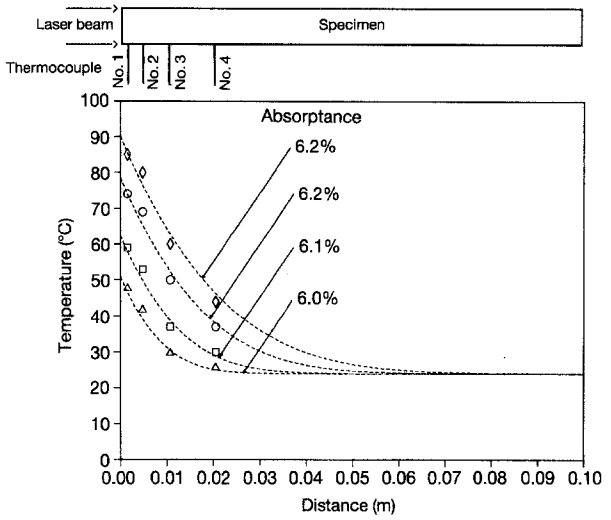

Figure 11 Measured temperature, simulated temperature and calculated absorptances as a function of laser irradiation time for one-dimensional SM45C steel specimen (laser power, 48 W). For: (◇) 30 s, (○) 20 s, (□) 10 s and (△) 5 s.

and from 5 to 5.5% for SM45C steel when the laser beam power was 82 W and the irradiation time was increased from 2 to 8 s. The difference in absorptances between the one-dimensional and two-dimensional specimens for the same metals can be attributed to the local change of surface conditions, in addition to differences of laser power and irradiation time.

4.2. High power laser beam for melting specimen

The same method was used to obtain laser absorptance, even though the laser power was high enough to melt the specimen's surface. If the laser irradiation time was so short that the specimen temperature was not high enough, the calculated temperatures that were obtained by using a single absorptance agreed well with those measured experimentally. If the laser

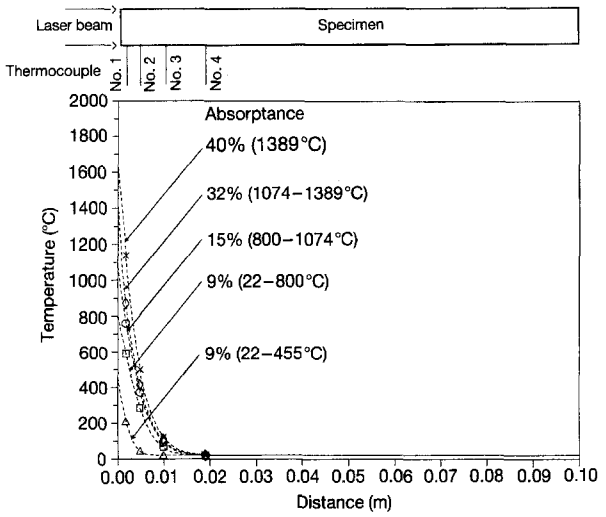

Figure 12 Measured temperature, simulated temperature and sequential calculated absorptances for one-dimensional STS304 stainless steel specimen (laser power, 760 W). For: (×) 5.75 s, (◇) 5.25 s, (○) 5 s, (□) 4 s and (△) 1 s.

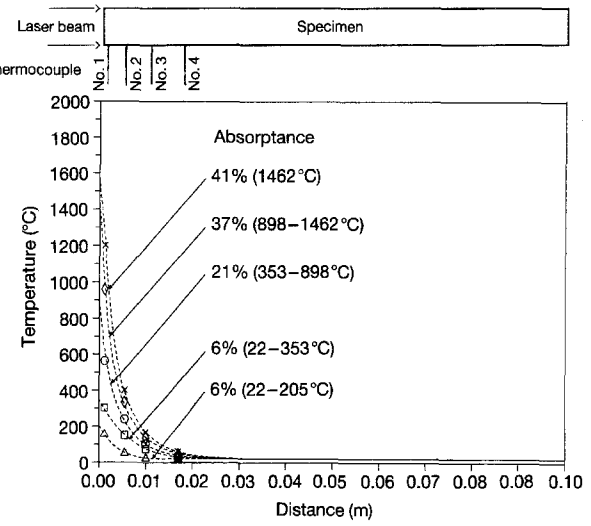

Figure 13 Measured temperature, simulated temperature and sequential calculated absorptances for one-dimensional SM45C steel specimen (laser power, 720 W). For: (×) 5.5 s, (◇) 5 s, (○) 4 s, (□) 3.25 s and (△) 1 s.

irradiation time was extended, then the specimen temperature increased rapidly, and also absorptance increased to a large value. In this case the calculated temperature distribution deviated much from the measured one if a single absorptance value was used throughout the whole temperature range. Therefore, if the specimen temperature was very high, it was divided by several temperature intervals, and average absorptance was assumed in each temperature range. Thus, a series of arbitrary absorptances were used as boundary conditions in each range to calculate temperature distribution, until this fitted well with the experimentally measured temperature.

Fig. 12 shows the temperature distributions for rod-shaped STS304 stainless steel when the laser power was 760 W and irradiation time was 1–5.75 s. As shown on this figure, the measured temperature distribution fitted well with the calculated one until the specimen temperature reached 800 °C (i.e. laser irradiation for 4 s), in which absorptance was assumed to be 9% in the computer program. If the laser irradiation time was 5 s, the specimen surface temperature was 1074 °C. In this case the measured temperature distribution did not fit the calculated one if the same single absorptance value was used from room temperature to 1074 °C in the computer program. However, if the absorptance was chosen to be 9% from room temperature to 800 °C and averaged 15% from 800 to 1074 °C for boundary conditions in the numerical calculation, the calculated temperature distribution fitted well with the experimentally measured one. After laser irradiation for 5.25 s, the surface temperature reached 1374 °C. In this case, if average absorptances were chosen as 9% from room temperature to 800 °C, 15% from 800 to 1074 °C, and 32% from 1074 to 1374 °C in the boundary conditions, then the calculated temperature distribution fitted well with the experimentally measured one. In the same way, the laser beam absorptance was calculated as 40% at the melted surface of STS304 stainless steel.

Fig. 13 shows the temperature distribution for the rod-shaped SM45C steel specimen, when the CO_2 laser beam of 720 W was irradiated from 1 to 5.5 s. Laser absorptance was calculated as 6% until the surface temperature reached 353 °C. As the temperature increased by extending laser irradiation, the absorptance values increased further. In the same way as mentioned above, if the laser absorptance was chosen to be 6% from room temperature to 353 °C, 21% from 353 to 898 °C, 37% from 898 to 1462 °C, and 41% in the melted surface for boundary conditions, the calculated temperature distribution fitted well with the experimentally measured one.

Figs 14 and 15 show the temperature distributions for the thin plate-shaped STS304 stainless steel specimen and SM45C steel specimen when a CO_2 laser beam of 720 W was irradiated for 1.7 and 1.3 s, respectively.

The calculated temperature distribution was obtained by the same method as mentioned for the one-dimensional specimen, and it fitted well with the experimentally measured one. Although the calculated temperature on the surface was above the effective range of the K-type thermocouple, this thermocouple was located a short distance away from the laser irradiated spot. Thus, the maximum measured temperature was far below the melting point and it belonged to the effective range of the K-type thermocouple. Above the melting point of the specimen, either the sharp edge became round, due to surface tension from the one-dimensional specimen, or a hole was pierced at the centre of the laser irradiated spot for the two-dimensional specimen. If the laser irradiation time was too long, either No. 1 thermocouple fell down for the one-dimensional specimen, or the laser beam passed through a hole for the two-dimensional specimen. Then, the temperature of that thermocouple dropped suddenly. Thus, this method cannot be applied far above the melting point.

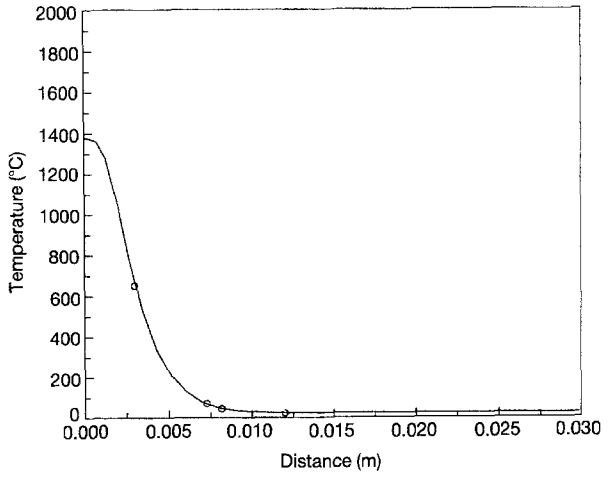

Figure 14 Measured (○) and predicted (—) temperatures for two-dimensional STS304 stainless steel specimen (laser power, 700 W; irradiation time, 1.7 s). Absorptances used in each temperature interval: 22–371 °C, 12.8%, 22–524 °C, 12.8%; 22–650 °C, 12.8%; 650–800 °C, 19.0%; 800–1399 °C, 22.0%; + 1399 °C, 41.0%.

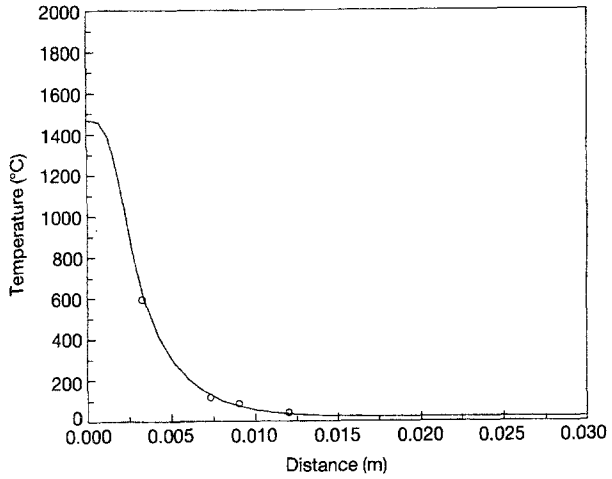

Figure 15 Measured (○) and predicted (—) temperatures for two-dimensional SM45C steel specimen (laser power, 700 W; irradiation time, 1.3 s). Absorptances used in each temperature interval: 22–101 °C, 5.5%; 22–240 °C, 5.5%; 240–600 °C, 20.5%; 600–1000 °C, 23.5%; 1000–1461 °C, 30.0%; + 1461 °C, 41.0%.

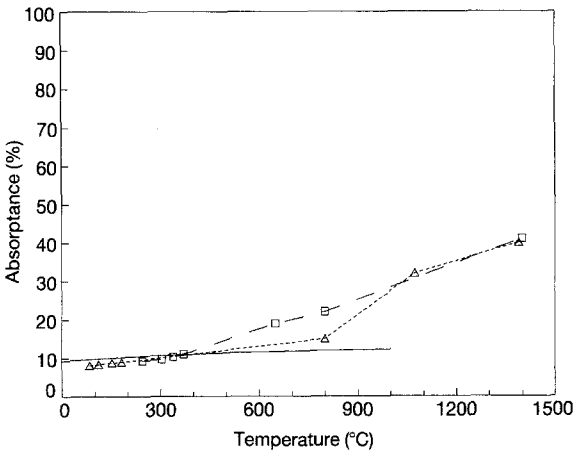

Figure 16 CO_2 laser beam absorptance as a function of temperature for STS304 stainless steel: (—) Hagen–Rubens solution, (△) one-dimensional finite difference method solution, (□) two-dimensional finite difference method.

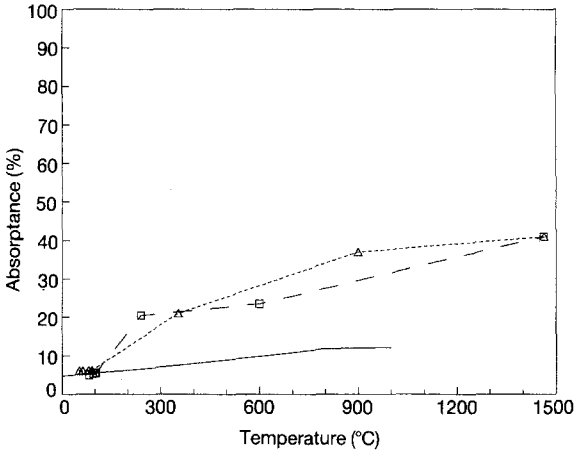

Figure 17 CO_2 laser beam absorptance as a function of temperature for SM45C steel: (—) Hagen–Rubens solution, (△) one-dimensional finite difference method solution, (□) two-dimensional finite difference method.

Figs 16 and 17 show the laser beam absorptances of STS304 stainless steel and SM45C steel as functions of temperature for the one-dimensional and two-dimensional cases.

As the temperature increased from room temperature to melting point, laser beam absorptances increased from 9 to 41% for STS304 stainless steel and from 5 to 41% for SM45C steel. Here, the solid line represents the theoretical CO_2 laser beam absorptance calculated by the Hagen–Rubens equation, while the dotted and dashed lines represent absorptances calculated by the one-dimensional and two-dimensional numerical methods. Electrical resistivities of both metals did not change much with increasing temperature, unless phase transformations did not occur [21]. Although the STS304 stainless steel has f.c.c. structure from room temperature to melting point, SM45C steel transforms from b.c.c. structure to f.c.c. near 800 °C. Thus the absorptance of STS304 stainless steel increased linearly with increasing specimen temperature, while that of SM45C steel changed slightly from 800 °C.

In these figures, although the calculated absorptances agreed well with theoretical values at low temperature, they increased very much from 800 °C for STS304 stainless steel and 300 °C for SM45C steel. In order to find out the reason why they increased from these temperatures, TGA–DTA experimental work was carried out for both specimens. According to these results, oxidation took place from 700 °C for STS304 stainless steel and at 300 °C for SM45C steel. The CO_2 laser beam absorptance is quite high on oxide compared with that on pure metal. Therefore, one reason why CO_2 laser absorptance increased drastically near 800 and 300 °C was attributed to the formation of an oxide layer on the specimen. Another reason may be the addition of reaction heat from oxidation, especially for SM45C steel.

If the temperature is high enough on the metal surface during laser irradiation, gas pressure due to

evaporation, and gas expansion tend to form a keyhole [22]. If a keyhole is formed on the specimen, the laser beam is absorbed very much due to multiple reflection and absorption effects. Many investigators' results, as shown in Table I, may indicate enhanced absorptances due to multiple reflection and absorption effects in the keyhole. However, since the maximum temperature in the specimen was just above melting point in this work, keyhole formation was avoided, and the multiple absorption effect would not be expected. According to Figs 16 and 17, although absorptances of both metals were different at relatively low temperatures, they had almost the same values at their melting temperatures. Therefore, the absorptance of the CO_2 laser beam on various steels can be assumed to be about 41%. The reason considered is that they have quite different electrical resistivities due to their compositions and structures at low temperature. However, if the metals melt at high temperature, their structures become amorphous phases and thus the effect of different structures on electrical resistivity disappears above the melting point.

5. Conclusions

CO_2 laser beam absorptances were obtained for one-dimensional and two-dimensional specimens using a modified finite difference method. Temperature dependence of thermal properties and heat loss due to convection were taken into account in these numerical calculations. Increasing the specimen temperature from room temperature to melting point, calculated absorptances were from 8 to 41% for STS304 stainless steel and from 5 to 41% for SM45C steel, respectively. At low temperatures, although absorptances differed little between the one-dimensional and two-dimensional specimens, these values were very close to theoretical values calculated from the electrical resistivities of specimens. Above 800 °C for STS304 stainless steel and 300 °C for SM45C steel, absorptances increased considerably due to the formation of an oxide layer on the specimen.

Both absorptances for the one-dimensional and two-dimensional cases showed the same value of 41% at their melting point for STS304 stainless steel and SM45C steel, in which the structure of both specimens became amorphous phase.

Acknowledgements

This work was supported by KOSEF (NO. 90-04-00-02).

References

1. T. J. WIETING and J. L. DeROSA, J. Appl. Phys. **50**(2) (1979) 1071.
2. C. BANAS, in "The Industrial Laser Annual Handbook", edited by D. Belforte and M. Levitt (PennWell, Tulsa, OK, 1986) p. 69.
3. G. HERZIGER, *ibid.* p. 108.
4. I. MIYAMOTO, H. MARUO and Y. ARATA, in "Laser Processing Fundamentals, Applications and System Engineering", SPIE Vol. 668, edited by W. W. Duley and R. Weeks, (International Society of Optical Engineering, Bellingham, 1986). p. 11.
5. D. T. SWIFT-HOOK and A. E. F. GICK, *Weld. J.* **52**(11) (1973) 492.
6. A. S. KAYE, A. G. DELPH and C. J. NICOLSON, *Appl. Phys. Lett.* **43**(5) (1983) 142.
7. D. W. MOON and E. A. METZBOWER, in "Proceedings of the International Power Beam Conference, Columbus", edited by E. A. Metzbower and D. Hausner, (American Society for Metals, Metals Park, OH, 1988) p. 125.
8. E. A. METZBOWER, *ibid.* p. 141.
9. T. H. KIM and J. G. KIM, *J. Mater. Sci. Lett.* **11** (1992) 1263.
10. T. H. KIM, C. E. ALBRIGHT and S. CHIANG, *J. Laser Appl.* **2** (1990) 23.
11. K. C. CHONG, MSc Thesis, Yonsei University, Seoul 1991.
12. B. Y. YOO, MSc Thesis, Yonsei University, Seoul 1991.
13. F. P. INCROPERA and D. P. DeWITT, "Introduction to Heat Transfer" (Wiley, New York, 1985) p. 177.
14. J. MAJUMDAR and W. M. STEEN, *J. Appl. Phys.* **51**(2) (1980) 941.
15. A. F. A. HOADLEY, M. RAPPAZ and W. ZIMMERMANN, *Metal. Trans. B.* **22B** (1991) 101.
16. S. KUO and Y. LE, *Metal. Trans. A.* **14A** (1983) 2245.
17. J. P. HONG, "Numerical Analysis of Heat Conduction and Diffusion" (Bando Publishing Co. Seoul, 1991) (in Korean) p. 75.
18. R. D. PEHLKE, A. JEYARAJAN and H. WADA, "Summary of Thermal Properties for Coating Alloys and Mold Materials" (University of Michigan, 1982) p. 25.
19. R. E. HUMMEL, "Electronic Properties of Materials" (Springer-Verlag, 1985) p. 137.
20. W. W. DULEY, "Laser Processing and Analysis of Materials" (Plenum, New York, 1983) p. 70.
21. Special Steels, (Collected data by KISCO, 1978) (in Korean).
22. T. H. KIM, *J. Mater. Sci. Lett.* **10** (1991) 400.

Received 9 September 1993
and accepted 6 July 1994